Inferring terrestrial photosynthetic light use efficiency of temperate ecosystmes from space

Inferring terrestrial photosynthetic light use efficiency of temperate ecosystems from space

Thomas Hilker,[1,2] Nicholas C. Coops,[1] Forrest G. Hall,[2,3] Caroline J. Nichol,[4] Alexei Lyapustin,[2,3] T. Andrew Black,[5] Michael A. Wulder,[6] Ray Leuning,[7] Alan Barr,[8] David Y. Hollinger,[9] Bill Munger,[10] and Compton J. Tucker[2]

Received 18 February 2011; revised 20 April 2011; accepted 4 May 2011; published 29 July 2011.

[1] Terrestrial ecosystems absorb about 2.8 Gt C yr^{-1}, which is estimated to be about a quarter of the carbon emitted from fossil fuel combustion. However, the uncertainties of this sink are large, on the order of ±40%, with spatial and temporal variations largely unknown. One of the largest factors contributing to the uncertainty is photosynthesis, the process by which plants absorb carbon from the atmosphere. Currently, photosynthesis, or gross ecosystem productivity (GEP), can only be inferred from flux towers by measuring the exchange of CO_2 in the surrounding air column. Consequently, carbon models suffer from a lack of spatial coverage of accurate GEP observations. Here, we show that photosynthetic light use efficiency (ε), hence photosynthesis, can be directly inferred from spaceborne measurements of reflectance. We demonstrate that the differential between reflectance measurements in bands associated with the vegetation xanthophyll cycle and estimates of canopy shading obtained from multiangular satellite observations (using the CHRIS/PROBA sensor) permits us to infer plant photosynthetic efficiency, independently of vegetation type and structure ($r^2 = 0.68$, compared to flux measurements). This is a significant advance over previous approaches seeking to model global-scale photosynthesis indirectly from a combination of growth limiting factors, most notably pressure deficit and temperature. When combined with modeled global-scale photosynthesis, satellite-inferred ε can improve model estimates through data assimilation. We anticipate that our findings will guide the development of new spaceborne approaches to observe vegetation carbon uptake and improve current predictions of global CO_2 budgets and future climate scenarios by providing regularly timed calibration points for modeling plant photosynthesis consistently at a global scale.

Citation: Hilker, T., et al. (2011), Inferring terrestrial photosynthetic light use efficiency of temperate ecosystems from space, *J. Geophys. Res.*, *116*, G03014, doi:10.1029/2011JG001692.

1. Introduction

[2] The net carbon exchange of terrestrial ecosystems is dominated by GEP and respiration [*Valentini et al.*, 2000], both of which are in the order of about 60 Gt yr^{-1}. GEP is the product of photosynthetically active radiation (PAR) incident upon the canopy, the fraction of it being absorbed by photosynthetically active vegetation elements (green f_{PAR} referred to hereafter as f_{PAR}) and the efficiency (ε) with which plants can use this absorbed radiation energy to produce biomass [*Monteith*, 1977]. While f_{PAR} and PAR can be readily determined from remote sensing observations globally [*Myneni and Williams*, 1994; *Sellers et al.*, 1994; *Van Laake and Sanchez-Azofeifa*, 2005], direct inference of ε has not yet been possible [*Hilker et al.*, 2008a; *Rahman et al.*, 2001]. Light use efficiency is determined by the most limiting of a large number of variables restraining the photochemical reaction process and, as a result, varies widely both in space and time. Under optimal conditions, most of the absorbed radiation energy will be directed toward the reaction center of Photosystem (PS) II, where it is used to produce photosynthate by fixing CO_2 from the surrounding air column. When photosynthesis is limited by water availability, nutrients or temperatures, excess radiation

[1]Faculty of Forest Resources Management, University of British Columbia, Vancouver, British Columbia, Canada.
[2]NASA Goddard Space Flight Center, Greenbelt, Maryland, USA.
[3]Joint Center for Earth Systems Technology, University of Maryland, Baltimore County, Baltimore, Maryland, USA.
[4]School of GeoSciences, University of Edinburgh, Edinburgh, UK.
[5]Land and Food Systems, University of British Columbia, Vancouver, British Columbia, Canada.
[6]Canadian Forest Service, Victoria, British Columbia, Canada.
[7]CSIRO Marine and Atmospheric Research, Canberra, Australia.
[8]Climate Research Branch, Environment Canada, Saskatoon, Saskatchewan, Canada.
[9]Northern Research Station, U.S. Forest Service, Durham, New Hampshire, USA.
[10]Department of Earth and Planetary Sciences, Harvard University, Cambridge, Massachusetts, USA.

0148-0227/11/2011JG001692

energy is dissipated thermally by means of protective leaf pigments: Triggered by the acidification of the thylakoid membrane, the xanthophyll cycle pigment violaxanthin is converted rapidly via intermediate antheraxanthin to zeaxanthin [*Demmig-Adams and Adams*, 1996]. This process is reversed when light limits photosynthesis [*Demmig-Adams and Adams*, 1996; *Demmig-Adams*, 1998].

[3] Remote sensing of GEP and hence ε in a spatially contiguous mode has been a long-term goal of Earth and climate change research seeking universal, generic modeling approaches of plant productivity applicable across multiple biomes and a wide variety of vegetation types. Numerous studies [*Fuentes et al.*, 2006; *Gamon et al.*, 1992; *Gamon et al.*, 1997; *Meroni et al.*, 2008; *Nichol et al.*, 2000] have related ε to the photochemical reflectance index (PRI), a narrow wave band spectral index that is directly associated with changes in the xanthophyll cycle, but the dependency of PRI on extraneous effects such as canopy structure, reflectance from nonphotosynthetic background, the ratio of chlorophyll to carotenoid content [*Stylinski et al.*, 2002; *Nakaji et al.*, 2006] and the Sun-observer geometry have hampered its use at canopy, landscape and global scales for almost two decades. At the leaf scale, nonphotochemical quenching is primarily a function of the degree of leaf illumination [*Demmig-Adams*, 1998]: In cases where GEP is limited by factors other than light ($\varepsilon < \varepsilon_{max}$), ε is closely related to canopy shadow fractions (α_s) [*Hall et al.*, 2008; *Hilker et al.*, 2008b, 2008c]. This is due to the fact that sunlit leaves are more likely to be exposed to excess radiation levels than shaded leaves. However, this relationship disappears under conditions where light is limiting GEP ($\varepsilon_{canopy} = \varepsilon_{max}$), as in this case, photosynthesis will, by definition, not be down regulated in either sunlit or shaded leaves ($\varepsilon_{sunlit} = \varepsilon_{shaded} = \varepsilon_{max}$). As a result, the slope of the relationship between ε and α_s is proportional to canopy light use efficiency [*Hall et al.*, 2008, 2011; *Hilker et al.*, 2010].

[4] This concept has two important implications for remote sensing of ε using PRI. First, stand-level ε cannot be observed from traditional, monoangle observations because the proportion of α_s observed by the sensor at a given time may not be representative of the canopy and the contribution of α_s to the photosynthetic down regulation is unknown. Second, multiangular measurements of PRI can be used to determine stand level ε if α_s is known for each view angle. This second proposition is true because under the assumption of singular leaf scattering, which is reasonable for remote sensing of wavelengths in the visible bands, a normalized difference reflectance index cannot change its value with the viewing geometry unless the value of one of its bands changes as a physiological response of the degree of leaf illumination [*Hall et al.*, 2008]. Based on these two principles it can be concluded that the first derivative of PRI with respect to shadow fractions ($\Delta PRI\ \Delta\alpha_s^{-1}$ or PRI') can be used to infer instantaneous ε at the canopy level [*Hilker et al.*, 2010].

[5] In this paper, we demonstrate our approach, which has been shown analytically by *Hall et al.* [2011], from space using multiangular, satellite observations acquired by the Compact High Resolution Imaging Spectrometer (CHRIS) sensor on board European Space Agency's Project for On-Board Autonomy (PROBA) research satellite. The objective of this study was to compare spaceborne measurements of PRI' with eddy covariance (EC) observations of ε acquired across a number of forest types with different structure and physiology, and to demonstrate the usability of PRI' as a generic technique for inferring ε across these different biomes from satellite data.

2. Site Description

[6] To demonstrate the robustness of our approach, eight different sites were selected based on the availability of simultaneous CHRIS/PROBA satellite data and eddy flux tower observations. Although data were not available for some important ecosystems such as tropical sites, the ecosystems that were sampled cover a wide range of forest age classes and temperate ecosystem types from boreal needleleaf to wet temperate eucalypt forests; an overview and site description is given in Table 1. Figure 1 shows a map of the various site locations; the structural differences of the test sites used in this study are illustrated in Figure 2. The forest structure across the different sites ranged from recent regeneration planted after harvest (HJP2002) to mature, coniferous (e.g., DF-49) and broadleaf (e.g., Harvard) forest stands. Figure 2 also illustrates the different stand densities and associated background reflectance visible from optical data, which is lower for the denser forest stands (e.g., Figures 2a and 2b) but higher especially in cases in Figures 2d, 2g and 2h.

3. Methods

3.1. Eddy Flux Observations

[7] Canopy GEP was determined from eddy covariance data acquired from the data archive of the Canadian Carbon Program (CCP) for the Canadian sites, Ameri-Flux for the U.S. sites, and Ozflux for the Australian site (Table 1). Net ecosystem exchange (NEE) was determined as the sum of the half-hourly fluxes of CO_2 and the rate of change in CO_2 storage in the air column between ground and EC measurement level [*Barr et al.*, 2004]. In case of the Harvard and Tumbarumba sites, fluxes were available as hourly observations [*Horii et al.*, 2004; *Leuning et al.*, 2005]. Incident and reflected PAR (μmol m^{-2} s^{-1}) was measured from upward and downward looking quantum sensors above and below the canopy, and f_{PAR} was derived at each site from the incident and reflected total PAR measured above and below the canopy ($\rho_1(\theta)$ and $\rho_2(\theta)$), the effective leaf area index (L_e), and the solar zenith angle (θ) at the time of measurement [*Chen*, 1996; *Chen et al.*, 2006].

$$f_{PAR} = [1 - \rho_1(\theta)] - [1 - \rho_2(\theta)] \exp\left(\frac{G_t(\theta) LAI_e}{\cos\theta}\right) \quad (1)$$

where $G_t(\theta)$ is the projection coefficient for total PAR transmission, approximated as a constant of 0.5. (Please note that this an approximation, as f_{PAR} refers to "green f_{PAR}" [*Chen*, 1996].)

[8] Gross ecosystem production was determined as the difference between net ecosystem exchange (NEE) and daytime ecosystem respiration (R_D) [*Humphreys et al.*,

Table 1. Site Description

Site	Reference	Latitude, Longitude (deg)	Elevation (m)	Dominant Species	Leaf Area Index	Age (years)	Height (m)	Annual Mean Temperature (°C)
DF-49	*Morgenstern et al.* [2004]	−125.334, 49.867	340	*Pseudotsuga menziesii*, *Thuja plicata*, *Tsuga heterophylla*	7.1	60	35	8.1
Harvard	*Staebler and Fitzjarrald* [2005]	−72.171, 42.537	340	*Quercus rubra*, *Acer rubrum*, *Betula lenta*, *Pinus strobes*, *Tsuga canadensis*	3.4	80	23	8.3
HJP1975	*Amiro et al.* [2006], *Chen et al.* [2006], and *Schwalm et al.* [2006]	−104.645, 53.876	570	*Pinus banksiana*	1.4	35	6	0.4
HJP2002	*Amiro et al.* [2006], *Chen et al.* [2006], and *Schwalm et al.* [2006]	−104.649, 53.908	560	*Pinus banksiana*	0.9	8	0.1	0.4
Howland	*Xiao et al.* [2005]	−68.740, 45.204	60	*Picea rubens*, *Tsuga canadensis*	5.3	109	20	6.7
NOBS	*Bergeron et al.* [2007]	−98.481, 55.880	259	*Picea mariana*	4.8	160	9	−4.4
OJP	*Amiro et al.* [2006], *Chen et al.* [2006], and *Schwalm et al.* [2006]	−104.692, 53.916	579	*Pinus banksiana*	2	91	13	0.4
Tumbarumba	*Leuning et al.* [2005]	148.152, −35.656	1000	*Eucalyptus delegatensis*, *Eucalyptus dalrymplean*	1.4	90	40	8.0

2006]. R_D was calculated using the annual exponential relationship between nighttime NEE and soil temperature at 5 cm depth after applying a logarithmic transformation to correct for heteroscedasticity [*Black et al.*, 1996; *Goulden and Crill*, 1997]. Finally, ε as defined by *Monteith* [1972, 1977], can be described as the ratio of the photosynthetic net output (GEP) divided by the energy input into the photosynthetic system:

$$\varepsilon = \frac{\mathrm{GEP}}{\mathrm{PAR} \times f_{\mathrm{PAR}}} \tag{2}$$

More detailed descriptions on processing of the eddy covariance data are given, for instance, by *Humphreys et al.* [2006] and *Leuning et al.* [2005]; a comprehensive review on fluxnet procedures and processing of EC data is provided by *Baldocchi et al.* [2001].

3.2. CHRIS/PROBA Imagery

[9] CHRIS is an imaging spectrometer with a 615 km Sun-synchronous orbit and an orbital repeat cycle of approximately 7 days. Its maximum spatial resolution is 18 m or 34 m at nadir, depending on the mode setting, with a swath width of 14 km. The CHRIS/PROBA configuration permits along-track narrow-band spectrometric observations of PRI of up to five angles (+55°, +36°, 0°, −36°, −55°). This data is acquired nearly simultaneously within each overpass during which stand level ε may be considered constant. As a demonstration instrument, CHRIS/PROBA provides areal coverage for a limited number of predefined

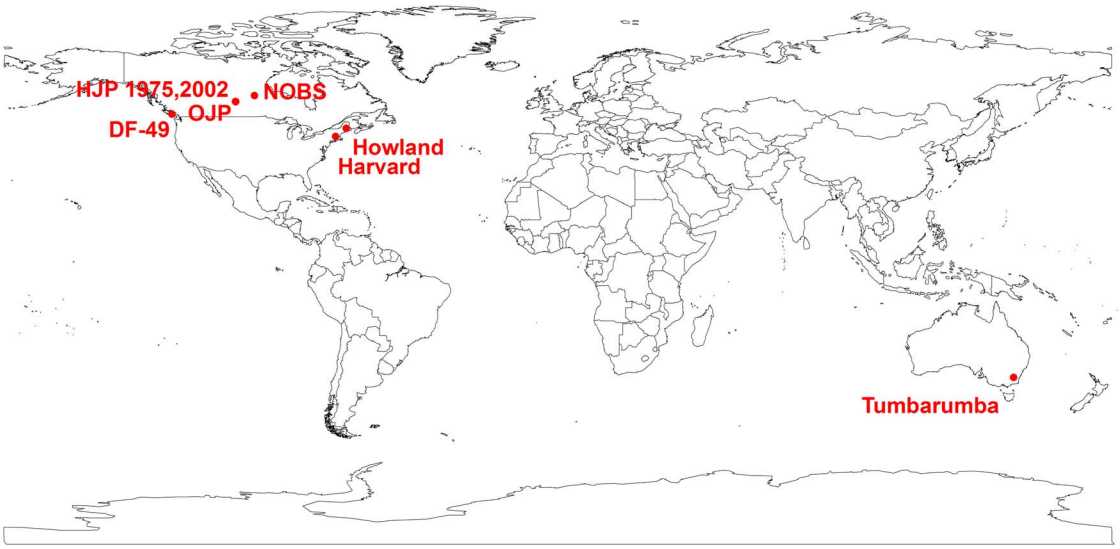

Figure 1. Location of the selected research sites. CHRIS/PROBA and eddy flux data were collected simultaneously between the years 2002 and 2008.

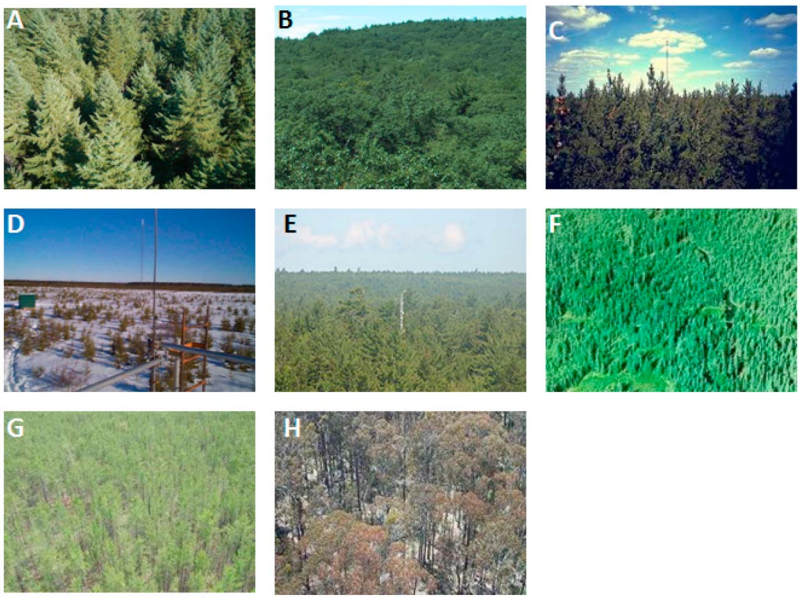

Figure 2. Structural differences at the eight research sites presented in this study. The sites are (a) DF-49, (b) Harvard Forest, (c) HJP1975, (d) HJP2002, (e) Howland Forest, (f) NOBS, (g) OJP and (h) Tumbarumba.

sites [*Fletcher*, 2004]. CHRIS/PROBA images obtained from ESA's online archive (https://oa-es.eo.esa.int/ra/) were acquired between 2001 and 2009.

[10] Acquisitions having simultaneous EC flux data were selected to represent as wide a range of different structural types as possible to evaluate the ecosystem robustness of the concept. No available observations were excluded from this analysis. CHRIS data can be acquired in different modes to allow data collection with variable wave bands and bandwidths. For this study, CHRIS data collected in modes 1 and 3 were used, as they provided the appropriate PRI wave bands at around 531 and 570 nm. The satellite observations were preprocessed using the VISAT tool of the European Space Agency to reduce data noise [*Gómez-Chova et al.*, 2008], to convert satellite measured radiance to top of atmosphere reflectance, and to screen the images for clouds [*Thuillier et al.*, 2003].

[11] Satellite observed reflectance depends on two main parameters, aerosol optical thickness (AOT) and the bidirectional reflectance function (BDRF). Appropriate algorithms to deal accurately and simultaneously with both BDRF and the effects of aerosols on path scattering have yet to be developed for CHRIS/PROBA. Most commonly a Lambertian surface model is used [*Hilker et al.*, 2009]. While this step simplifies processing, the Lambertian assumption reduces anisotropy of derived surface reflectance with the error dependent on the viewing geometry [*Lyapustin et al.*, 2007]. *Hilker et al.* [2009] showed that this assumption directly contradicts the multiangle effects observed in PRI and consequently, no meaningful multiangular observations of PRI can be obtained from single orbit atmospheric corrections [*Hilker et al.*, 2009]. Our previous work has also demonstrated that this challenge could be overcome when using multiple acquisitions over time for which the retrieval of aerosol optical thickness does not require these simplifying assumptions [*Hilker et al.*, 2009; *Lyapustin et al.*, 2007]; however, no such algorithm currently exists for CHRIS/PROBA. From theoretical considerations, it can be shown that the error associated with atmospheric effects is mostly a function of the range of shadow fractions viewed during an overpass. *Hall et al.* [2011] showed that aerosols tend to suppress the variation of PRI with shadow fraction and modify the relationship with LUE and further demonstrated that the PRI' − LUE relationship remains robust in spite of it. Clearly, an improved atmospheric correction technique for CHRIS/PROBA should further improve the relationships by mitigating atmospheric noise.

[12] Another critical issue for the use of CHRIS/PROBA observations is geometric correction of the multiangular data. First, images captured at large view angles are susceptible to resolution change and blurring, which makes the precise location of ground control points (GCPs) difficult, and second, local geometric distortion caused by topographic effects and/or platform instability can make rigid transformation models unreliable [*Ma et al.*, 2010]. Arguably, the most rigid approach for image registration at off-nadir angles are physical sensor models [*Leprince et al.*, 2007; *Toutin*, 2004], however, these models require reliable metadata on sensor target geometry which are not available for CHRIS/PROBA [*Shaker et al.*, 2008]. To compensate for this lack of information, we applied a two step georectification algorithm described by *Ma et al.* [2010] and registered CHRIS/PROBA satellite imagery with respect to Landsat observations of the same locations. First, common ground control points (GCPs) between Landsat and CHRIS/PROBA were automatically identified using a scale-invariant feature transform (SIFT) [*Lowe*, 2004]. SIFT is a method for extracting and matching distinctive features in image pairs invariant to image scale and rotation, across a substantial range of affine distortion, change in 3D viewpoint, addition of noise, and change in illumination [*Lowe*, 2004]. The network of these initial GCPs was then densified in a second

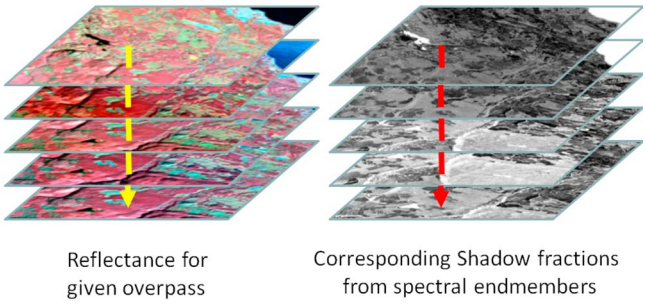

Figure 3. Acquisition of ΔPRI $\Delta\alpha_s^{-1}$ for a given CHRIS/PROBA overpass. PRI values and corresponding shadow fractions were obtained for each pixel of a stack of up to five multiangular observations acquired along track under conditions where stand level ε can assumed to be constant.

step using a normalized cross correlation (NCC) approach and CHRIS/PROBA images were warped by means of a nonreflective similarity transformation [*Goshtasby*, 1988]. For moderately undulated terrain, such as the case for most eddy covariance flux sites [*Baldocchi et al.*, 2001], this simple approach has been shown to yield geolocation accuracies within the subpixel range which should be sufficiently accurate for stand level observations [*Ma et al.*, 2010] given the spatial resolution of the CHRIS/PROBA data.

3.3. Computation of PRI'

[13] In previous studies [*Hall et al.*, 2008; *Hilker et al.*, 2009, 2010], canopy shadow fractions have been estimated from airborne light detection and ranging (lidar). While this approach has proven suitable to provide accurate measurements of mutual shading of individual stands [*Hilker et al.*, 2008b], the availability of lidar is limited, and, consequently, global estimates of PRI' will require alternative retrievals of α_s. One possibility is to derive α_s directly from the satellite imagery using spectral mixture analysis [*Hall et al.*, 1997, 1996, 1995; *Peddle and Smith*, 2005] thereby avoiding the need for a secondary data source. This technique also has the advantage that it only considers the shading associated with PRI. Various algorithms are available for spectral unmixing; in this study we used the sequential maximum angle convex cone (SMACC) model [*Gruninger et al.*, 2004]. The model defines spectral endmembers as vectors within a data set that cannot be represented by a positive linear combination of other vectors. An advantage of SMACC is that, as a nonsupervised classification technique, it allows automated extraction of canopy shading. To avoid overfitting the model, two end-members (sunlit leaves, sunlit background) were derived per CHRIS/PROBA scene, in addition to α_s (please note that shaded background was not explicitly extracted, as the PRI values as obtained from CHRIS/PROBA are also a composite of leaf and background reflectance). Shadow fractions were derived on a pixel-by-pixel basis for each image.

[14] PRI was computed from CHRIS/PROBA imagery as the normalized difference of CHRIS bands 4 (529 nm, bandwidth 12.9 nm) and 6 (569 nm, bandwidth 14.1 nm) for images acquired in CHRIS Mode 3 (all sites except for the southern BOREAS region), and band 11 (532 nm, bandwidth 13.4 nm) and 15 (573 nm, bandwidth 9.6 nm) for images acquired in CHRIS Mode 1 [*Gamon et al.*, 1992]. PRI and corresponding α_s were computed for each pixel of a multiangular image stack acquired during one overpass (see Figure 3). A single value of PRI' was derived from a simple linear regression model [*Hilker et al.*, 2010] for each overpass. In order to compare PRI' to EC derived ε, PRI' observations were then averaged in a radius of 150 m around the tower and half hourly ε was computed for each satellite overpass (satellite noon ± 15 min).

4. Results

[15] In total, images from 51 CHRIS/PROBA overpasses were acquired across all different sites with up to 5 cloud free, multiangular observations per overpass. The light use efficiency determined from the eddy covariance systems ranged from 0.01 g C MJ^{-1} to 0.96 g C MJ^{-1} across all different sites, Figure 4 shows a summary of EC-derived ε observed during all CHRIS/PROBA overpasses (satellite noon ± 15 min). Highest values of ε were observed for the Harvard and DF-49 sites, whereas ε was lowest at the harvested Jack pine site (HJP2002). These observations of the instantaneous LUE at the satellite overpass time likely differ from the average diurnal physiological conditions of each stand.

[16] Significant relationships were found between PRI and α_s across all sites; when observed under low levels of ε, the average coefficient of determination was $r^2 = 0.76$ ($p < 0.01$, $\varepsilon < 0.05$ g C MJ^{-1}). As theory predicts, the dependence of ε on α_s weakened with increasing ε, as PRI of sunlit and shaded canopy were more nearly equal. For instance, the mean coefficient of determination was $r^2 = 0.21$ for $\varepsilon > 0.25$; a summary of the strength of the relationship between PRI and α_s across all sites is given in Figure 5. Figure 6 illustrates the slope between PRI and α_s for four different levels of ε, using the HJP1975 site as an example, and contrasts these observations with potential canopy stress factors, notably pressure deficit (D) and temperature (T), observed from micrometeorological data (Figures 6e–6h). Figure 6 demonstrates the link between PRI' and environmental conditions. For instance, the slope between PRI and α_s was steepest when the physiological stress factors were highest (high D and T, Figures 6a and 6e). Only a moderate slope was found under a more relaxed state of the xanthophyll cycle (higher ε), while the relationship between PRI and α_s began to disintegrate (Figure 6d). Figure 6 also illustrates the correspondence between D, T, and PAR as major environmental factors on one side, and GEP as the physiological response on the other.

[17] The relationship between PRI' and ε derived from eddy covariance towers across all study sites is shown in Figure 7. Each data point represents the slope between PRI and α_s observed during one overpass (up to 5 different view angles). A strong, logarithmic relationship was found between EC-derived ε and PRI' obtained from the CHRIS/PROBA imagery ($r^2 = 0.68$, $p < 0.01$). Despite the notable differences in structure, species composition, climate and location, all observations followed the same nonlinear function derived theoretically by *Hall et al.* [2008] that showed this relationship to be insensitive to the unstressed

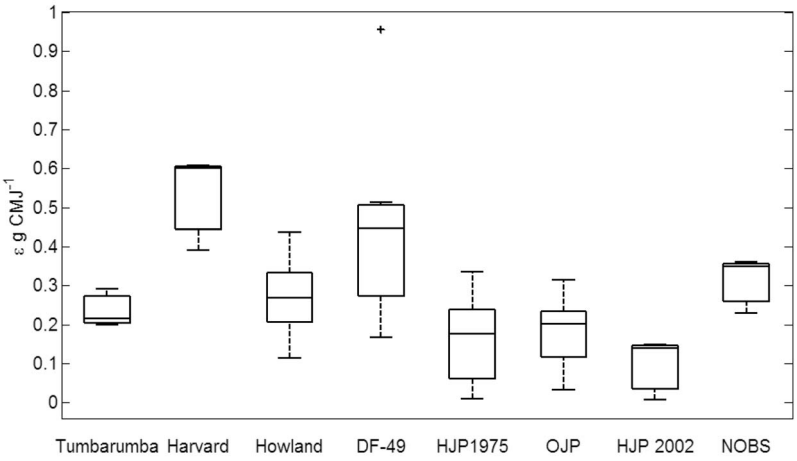

Figure 4. Range of variability in ε across the eight different test sites during the CHRIS/PROBA overpasses. All of these observations have been acquired at different times of the day during the satellite overpasses and are not representative of the physiological conditions of each stand (number of cloud-free observations: DF-49, n = 9; Harvard Forest, n = 3; HJP1975, n = 8; HJP2002, n = 8; OJP: n = 8; Howland Forest, n = 10; Tumbarumba, n = 3; NOBS, n = 3).

reflectance and structure of the vegetation, including background, thereby allowing the inference of ε across different biomes. For the biomes represented in this study, RMSE = 0.22 g C MJ^{-1}.

[18] The simultaneous acquisition of PRI and α_s from multiangular satellite imagery allowed, for the first time, a spatially explicit mapping of ε in those areas common to all multiangular images acquired during one overpass. Figure 8 shows the spatial distribution of an instantaneous value of ε. The location of the flux tower is shown in each map (please note that three southern Boreas sites (OJP, HJP1975, and HJP2002) were all contained in the same CHRIS/PROBA acquisition (Figure 8d)). The spatial variation across the different sites is clearly visible in Figure 8. Variations in ε were more pronounced at the denser coniferous sites (Figures 8a and 8c) than at the deciduous stands (Figure 8b). The largest differences in ε were found at the Tumbarumba site (Figure 8e). High light use efficiencies were observed for the irrigated pastureland (northwest), but low productivity was predicted for the nonirrigated, forested

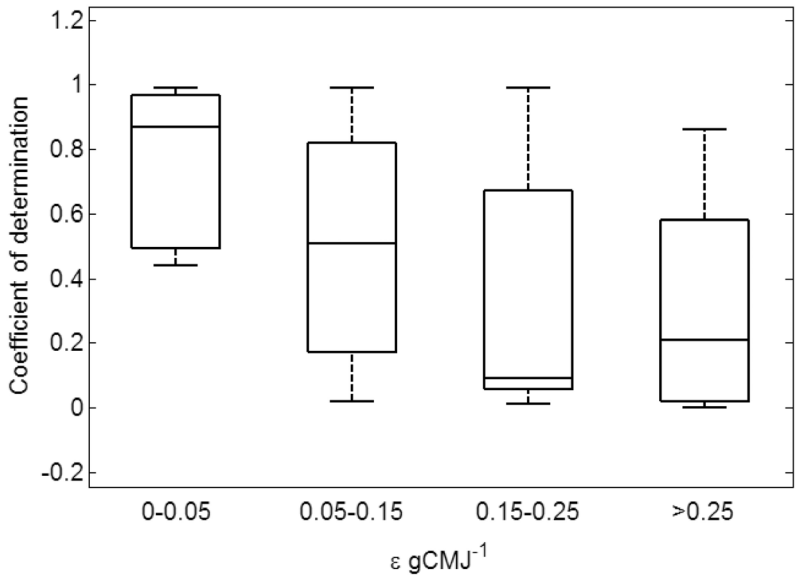

Figure 5. Box plot of the coefficient of determination (r^2) for the relationship between PRI and α_s across all sites grouped into different levels of EC-measured ε. Strong linear relationships were found for low levels of ε, but the relationship weakened for higher ε as PRI became less driven by canopy shadow fractions (number of observations: n = 6 ($\varepsilon < 0.05$), n = 17 ($0.05 < \varepsilon < 0.15$), n = 18 ($0.15 < \varepsilon < 0.25$), n = 10 ($\varepsilon > 0.25$)).

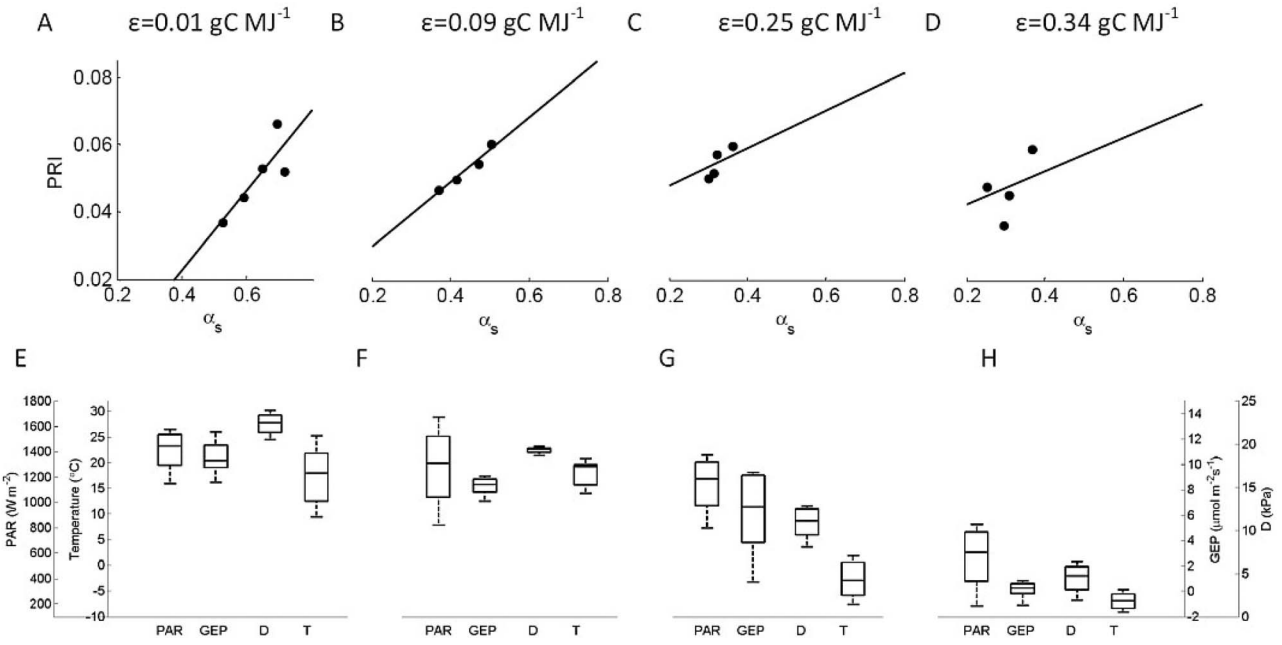

Figure 6. (a–d) Slope between PRI and α_s for four different levels of ε, here using HJP1975 as an example. (e–h) The corresponding environmental conditions including PAR, GEP, pressure deficit (D) and temperature (T) for the ε values presented in Figures 6a–6d. The relationship between PRI and α_s begins to disintegrate as ε approaches ε_{max}.

sites. The smallest variability of all sites was observed at the NOBS site.

5. Discussion

[19] This study has demonstrated the observation of vegetation ε and therefore photosynthesis in a spatially continuous mode from satellite observations. The results reported in here are also supported by theoretical work using radiative transfer theory [*Hall et al.*, 2008, 2011] and stand level optical data collected continuously over 3 years. *Hilker et al.* [2010] compared multiangular tower-based radiometer data acquired at the DF-49 site and a mature Aspen stand in central Saskatchewan and found the regression lines between PRI' and ε of both stands to fall within the 95% confidence interval of each other. While the relationship derived by *Hilker et al.* [2010, Figure 10] is very similar to the one presented in this study, both are not directly comparable because of (1) atmospheric effects, which have not been accounted for in this study, and (2) the different ways in which α_s was determined.

[20] CHRIS/PROBA is currently the only sensor in orbit that allows multiangular acquisitions of the PRI wave bands along track, that is, during one overpass. Previous studies have demonstrated that other sensors, including NASA's Moderate Resolution Imaging Spectroradiometer (MODIS) are also able to obtain xanthophyll sensitive measurements from different view angles [*Drolet et al.*, 2005, 2008; *Hilker et al.*, 2009]. However, a multiangular capability from MODIS is not possible during a single overpass, rendering the computation of ΔPRI $\Delta\alpha_s^{-1}$ impossible.

[21] While this study has successfully used CHRIS/PROBA to infer stand level ε across a range of forested vegetation types, the limitations of this sensor are also acknowledged. First, while the georegistration algorithm applied in this study yielded sufficiently accurate results to infer PRI and α_s from stacks of multiangular acquisitions (Figure 3), more sophisticated models will likely be required at least in mountainous and more rugged terrains [*Ma et al.*, 2010]. One such approach could be a rigorous orthorectification technique [*Toutin et al.*, 1992], but further research will be required to allow the application of such an approach in an automated fashion. Second, an appropriate atmospheric correction algorithm will be needed to account for the anisotropy of PRI reflectance and increase the observation accuracy of spaceborne measurements. One such algorithm that has yielded promising results for

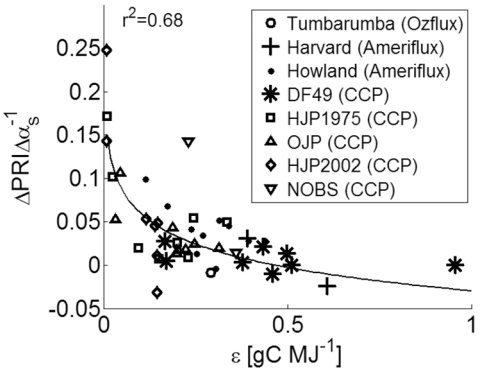

Figure 7. Relationship between ΔPRI $\Delta\alpha_s^{-1}$ (PRI') as observed from CHRIS/PROBA imagery and EC measured ε for the eight different research sites. The observations were taken between 2001 and 2009.

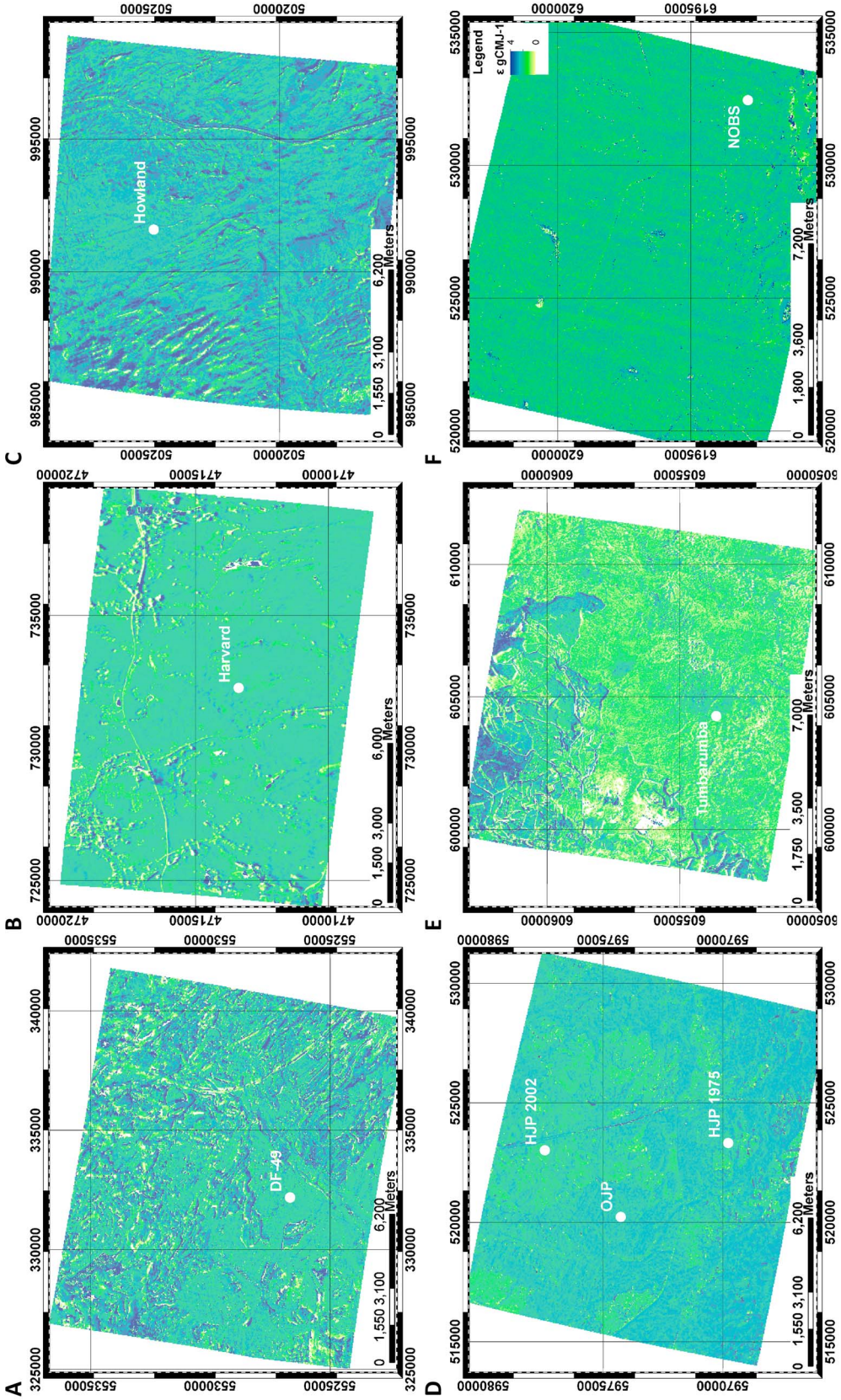

Figure 8. Maps of ε (in g C MJ^{-1}) as estimated from CHRIS/PROBA imagery using the relationship shown in Figure 7. The spatial variability in ε is apparent at all sites. At the Australian site, ε is also driven by availability of water, as the irrigated pasture shows significantly higher ε than the surrounding forest.

MODIS data is the multiangular implementation of atmospheric correction [*Lyapustin and Wang*, 2009]; however, adaptations will be necessary to allow the correction of finer spatial resolution (<100 m) along track observations obtained from CHRIS.

[22] Being a demonstration instrument, CHRIS/PROBA does not provide global coverage and data is limited to a few predefined locations, as the sensor was not designed to acquire and disseminate data on a regular schedule. As a result, the acquisition of spatially contiguous, high temporal frequency epsilon measurements desired to improve global GPP estimates, would require a new mission design. *Hall et al.* [2011] proposed a new, light-weight satellite platform to allow simultaneous acquisitions of f_{PAR}, PAR, and ε on a spatially contiguous basis at regular time intervals from space. The mission would permit a nearly simultaneous acquisition of PRI and NDVI wave bands from five angles and at a wide swath to allow global coverage with high temporal (daily) and moderate spatial (90 m) resolution.

[23] One of the advantages of PRI' rather than PRI is that PRI' is independent of extraneous effects (Figure 7). *Hall et al.* [2008, 2011] and *Hilker et al.* [2010] have shown theoretically and demonstrated experimentally that (1) nonphotosynthetic canopy elements do not contribute to PRI', because photosynthetic down regulation does not affect the PRI of nonphotosynthesizing canopy elements, (2) the measured differences in PRI between the sunlit and shaded photosynthetically active elements of the canopy are driven almost exclusively by the difference in ε, hence PRI, and (3) the relationship between PRI' and ε is largely independent of changes in canopy chemistry, e.g., the chlorophyll/carotenoid ratio [*Stylinski et al.*, 2002], because PRI' is insensitive to the unstressed leaf reflectance.

[24] While CHRIS/PROBA cannot be used in an operational sense, this satellite platform provides a unique opportunity to further test and develop the technique described in this study. Additional research is needed to investigate the use of PRI' across additional forested ecosystems, particularly the tropics, as well as nonforested vegetation types. Such sites could pose new challenges as the variability in shadow fractions is likely reduced due to a lack of structure. Likewise, the application of our approach to more heterogeneous stands also requires additional evaluation. An important aspect of satellite remote sensing of ε is that these observations will be skewed toward conditions where canopy epsilon is low, because they can only be acquired during sunny conditions. The potential implications for integrating sunny and cloudy periods across a range of sky diffuse fraction values in a modeling context need to be assessed in future research. An additional aspect for future research is to develop the science measurement and system design requirements for a space mission. Such missions may, for instance, benefit from observations acquired during the morning or later afternoon hours to facilitate the investigation of diurnal cycles and short-term vegetation responses.

[25] Global observation of GEP should significantly improve existing productivity and Earth system models [*Goetz and Prince*, 1998; *Running et al.*, 1999; *Potter et al.*, 1993; *Sellers et al.*, 1994, 1995] by providing the observations needed to both improve model biophysics, calibration and error assessment. For instance, PRI' observations could be used in a data assimilation approach to frequently assess and potentially correct the performance of vegetation growth models in a spatially explicit fashion. In addition, estimation of ε from PRI' will also help in understanding stress behavior in plants at the landscape level, thereby predicting ecosystem responses to a changing environment [*Sellers*, 1985].

6. Conclusion

[26] We have shown that along any orbital track, ε can be inferred from $\Delta\alpha_s\Delta PRI^{-1}$ with a logarithmic relationship across a wide assortment of forested biomes. The CHRIS/PROBA sensor provides a unique basis for further research. Ultimately a new space mission could infer PRI' at high temporal resolution globally, in a spatially contiguous mode. Adding additional spectral bands, such as the near infrared and red wavelengths, to such a satellite sensor to measure f_{PAR} would provide a direct estimate of GEP. We conclude that a new sensor design with the desired spatial coverage and revisit frequency to derive f_{PAR} and ε from multiple angles would allow up to daily observations of photosynthesis from space.

[27] **Acknowledgments.** The ESA CHRIS/PROBA images were provided by David G. Goodenough, Ray Merton, and Mathias Kneubühler, all principal investigators of the Evaluation and Validation of CHRIS (EVC) Project. This research is partially funded by the Canadian Carbon Program, the Natural Sciences and Engineering Research Council of Canada (NSERC) and BIOCAP, and an NSERC-Accelerator grant to N.C.C.

References

Amiro, B. D., et al. (2006), Carbon, energy and water fluxes at mature and disturbed forest sites, Saskatchewan, Canada, *Agric. For. Meteorol.*, *136*(3–4), 237–251, doi:10.1016/j.agrformet.2004.11.012.

Baldocchi, D., et al. (2001), Fluxnet: A new tool to study the temporal and spatial variability of ecosystem-scale carbon dioxide, water vapor, and energy flux densities, *Bull. Am. Meteorol. Soc.*, *82*(11), 2415–2434, doi:10.1175/1520-0477(2001)082<2415:FANTTS>2.3.CO;2.

Barr, A. G., T. A. Black, E. H. Hogg, N. Kljun, K. Morgenstern, and Z. Nesic (2004), Inter-annual variability in the leaf area index of a boreal aspen-hazelnut forest in relation to net ecosystem production, *Agric. For. Meteorol.*, *126*(3–4), 237–255, doi:10.1016/j.agrformet.2004.06.011.

Bergeron, O., H. A. Margolis, T. A. Black, C. Coursolle, A. L. Dunn, A. G. Barr, and S. C. Wofsy (2007), Comparison of carbon dioxide fluxes over three boreal black spruce forests in Canada, *Global Change Biol.*, *13*(1), 89–107, doi:10.1111/j.1365-2486.2006.01281.x.

Black, T. A., et al. (1996), Annual cycles of water vapour and carbon dioxide fluxes in and above a boreal aspen forest, *Global Change Biol.*, *2*(3), 219–229, doi:10.1111/j.1365-2486.1996.tb00074.x.

Chen, J. M. (1996), Canopy architecture and remote sensing of the fraction of photosynthetically active radiation absorbed by boreal conifer forests, *IEEE Trans. Geosci. Remote Sens.*, *34*(6), 1353–1368, doi:10.1109/36.544559.

Chen, J. M., A. Govind, O. Sonnentag, Y. Q. Zhang, A. Barr, and B. D. Amiro (2006), Leaf area index measurements at Fluxnet-Canada forest sites, *Agric. For. Meteorol.*, *140*, 257–268, doi:10.1016/j.agrformet.2006.08.005.

Demmig-Adams, B., and W. W. Adams (1996), The role of xanthophyll cycle carotenoids in the protection of photosynthesis, *Trends Plant Sci.*, *1*(1), 21–26, doi:10.1016/S1360-1385(96)80019-7.

Demmig-Adams, B. (1998), Survey of thermal energy dissipation and pigment composition in sun and shade leaves, *Plant Cell Physiol.*, *39*(5), 474–482.

Drolet, G. G., K. F. Huemmrich, F. G. Hall, E. M. Middleton, T. A. Black, A. G. Barr, and H. A. Margolis (2005), A MODIS-derived photochemical reflectance index to detect inter-annual variations in the photosynthetic light-use efficiency of a boreal deciduous forest, *Remote Sens. Environ.*, *98*(2–3), 212–224, doi:10.1016/j.rse.2005.07.006.

Drolet, G. G., E. M. Middleton, K. F. Huemmrich, F. G. Hall, B. D. Amiro, A. G. Barr, T. A. Black, H. A. McCaughey, and H. A. Margolis (2008), Regional mapping of gross light-use efficiency using MODIS spectral

indices, *Remote Sens. Environ.*, *112*, 3064–3078, doi:10.1016/j.rse.2008.03.002.

Fletcher, P. A. (2004), Image acquisition planning for the CHRIS sensor onboard PROBA, *Proc. SPIE, Int. Soc. Opt. Eng.*, *5546*, 141–148.

Fuentes, D. A., J. A. Gamon, Y. F. Cheng, H. C. Claudio, H. L. Qiu, Z. Y. Mao, D. A. Sims, A. F. Rahman, W. Oechel, and H. Y. Luo (2006), Mapping carbon and water vapor fluxes in a chaparral ecosystem using vegetation indices derived from AVIRIS, *Remote Sens. Environ.*, *103*(3), 312–323, doi:10.1016/j.rse.2005.10.028.

Gamon, J. A., J. Penuelas, and C. B. Field (1992), A narrow-waveband spectral index that tracks diurnal changes in photosynthetic efficiency, *Remote Sens. Environ.*, *41*(1), 35–44, doi:10.1016/0034-4257(92)90059-S.

Gamon, J. A., L. Serrano, and J. S. Surfus (1997), The photochemical reflectance index: an optical indicator of photosynthetic radiation use efficiency across species, functional types, and nutrient levels, *Oecologia*, *112*(4), 492–501, doi:10.1007/s004420050337.

Goetz, S. J., and S. D. Prince (1998), Variability in carbon exchange and light utilization among boreal forest stands: Implications for remote sensing of net primary production, *Can. J. For. Res.*, *28*(3), 375–389.

Gómez-Chova, L., L. Alonso, L. Guanter, G. Camps-Valls, J. Calpe, and J. Moreno (2008), Correction of systematic spatial noise in push-broom hyperspectral sensors: Application to CHRIS/PROBA images, *Appl. Opt.*, *47*(28), F46–F60, doi:10.1364/AO.47.000F46.

Goshtasby, A. (1988), Image registration by local approximation methods, *Image Vis. Comput.*, *6*(4), 255–261, doi:10.1016/0262-8856(88)90016-9.

Goulden, M. L., and P. M. Crill (1997), Automated measurements of CO_2 exchange at the moss surface of a black spruce forest, *Tree Physiol.*, *17*(8–9), 537–542.

Gruninger, J., A. J. Ratkowski, and M. L. Hoke (2004), The sequential maximum angle convex cone (SMACC) endmember model, in *Algorithms and Technologies for Multispectral, Hyperspectral, and Ultraspectral Imagery X*, edited by S. S. Shen and P. E. Lewis, *Proc. SPIE*, *5425*, 1–14.

Hall, F. G., Y. E. Shimabukuro, and K. F. Huemmrich (1995), Remote sensing of forest biophysical structure using mixture decomposition and geometric reflectance models, *Ecol. Appl.*, *5*(4), 993–1013, doi:10.2307/2269350.

Hall, F. G., D. R. Peddle, and E. F. Ledrew (1996), Remote sensing of biophysical variables in boreal forest stands of *Picea mariana*, *Int. J. Remote Sens.*, *17*(15), 3077–3081, doi:10.1080/01431169608949129.

Hall, F. G., D. E. Knapp, and K. F. Huemmrich (1997), Physically based classification and satellite mapping of biophysical characteristics in the southern boreal forest, *J. Geophys. Res.*, *102*(D24), 29,567–29,580, doi:10.1029/97JD02578.

Hall, F. G., T. Hilker, N. C. Coops, A. Lyapustin, K. F. Huemmrich, E. Middleton, H. Margolis, G. Drolet, and T. A. Black (2008), Multi-angle remote sensing of forest light use efficiency by observing PRI variation with canopy shadow fraction, *Remote Sens. Environ.*, *112*(7), 3201–3211, doi:10.1016/j.rse.2008.03.015.

Hall, F. G., T. Hilker, and N. C. Coops (2011), PHOTOSYNSAT, photosynthesis from space: Theoretical foundations of a satellite concept and validation from tower and spaceborne data, *Remote Sens. Environ.*, *115*, 1918–1925, doi:10.1016/j.rse.2011.03.014.

Hilker, T., N. C. Coops, M. A. Wulder, T. A. Black, and R. D. Guy (2008a), The use of remote sensing in light use efficiency based models of gross primary production: A review of current status and future requirements, *Sci. Total Environ.*, *404*(2–3), 411–423, doi:10.1016/j.scitotenv.2007.11.007.

Hilker, T., N. C. Coops, C. R. Schwalm, R. S. Jassal, T. A. Black, and P. Krishnan (2008b), Effects of mutual shading of tree crowns on prediction of photosynthetic light-use efficiency in a coastal Douglas-fir forest, *Tree Physiol.*, *28*(6), 825–834.

Hilker, T., N. C. Coops, F. G. Hall, T. A. Black, M. A. Wulder, Z. Nesic, and P. Krishnan (2008c), Separating physiologically and directionally induced changes in PRI using BRDF models, *Remote Sens. Environ.*, *112*(6), 2777–2788, doi:10.1016/j.rse.2008.01.011.

Hilker, T., A. Lyapustin, F. G. Hall, Y. Wang, N. C. Coops, G. Drolet, and T. A. Black (2009), An assessment of photosynthetic light use efficiency from space: Modeling the atmospheric and directional impacts on PRI reflectance, *Remote Sens. Environ.*, *113*(11), 2463–2475, doi:10.1016/j.rse.2009.07.012.

Hilker, T., et al. (2010), Remote sensing of photosynthetic light-use efficiency across two forested biomes: Spatial scaling, *Remote Sens. Environ.*, *114*, 2863–2874, doi:10.1016/j.rse.2010.07.004.

Horii, C. V., J. W. Munger, S. C. Wofsy, M. Zahniser, D. Nelson, and J. B. McManus (2004), Fluxes of nitrogen oxides over a temperate deciduous forest, *J. Geophys. Res.*, *109*, D08305, doi:10.1029/2003JD004326.

Humphreys, E. R., T. A. Black, K. Morgenstern, T. B. Cai, G. B. Drewitt, Z. Nesic, and J. A. Trofymow (2006), Carbon dioxide fluxes in coastal Douglas-fir stands at different stages of development after clearcut harvesting, *Agric. For. Meteorol.*, *140*(1–4), 6–22, doi:10.1016/j.agrformet.2006.03.018.

Leprince, S., S. Barbot, F. Ayoub, and J. P. Avouac (2007), Automatic and precise orthorectification, coregistration, and subpixel correlation of satellite images, application to ground deformation measurements, *IEEE Trans. Geosci. Remote Sens.*, *45*(6), 1529–1558, doi:10.1109/TGRS.2006.888937.

Leuning, R., H. A. Cleugh, S. J. Zegelin, and D. Hughes (2005), Carbon and water fluxes over a temperate Eucalyptus forest and a tropical wet/dry savanna in Australia: Measurements and comparison with MODIS remote sensing estimates, *Agric. For. Meteorol.*, *129*(3–4), 151–173, doi:10.1016/j.agrformet.2004.12.004.

Lowe, D. G. (2004), Distinctive image features from scale-invariant keypoints, *Int. J. Comput. Vis.*, *60*(2), 91–110, doi:10.1023/B:VISI.0000029664.99615.94.

Lyapustin, A., and Y. Wang (2009), *The Time Series Technique for Aerosol Retrievals Overland From MODIS*, Springer Praxis, Berlin.

Lyapustin, A., Y. Wang, R. Kahn, J. Xiong, A. Ignatov, R. Wolfe, A. Wu, B. Holben, and C. Bruegge (2007), Analysis of MODIS-MISR calibration differences using surface albedo around AERONET sites and cloud reflectance, *Remote Sens. Environ.*, *107*(1–2), 12–21, doi:10.1016/j.rse.2006.09.028.

Ma, J. L., J. C. W. Chan, and F. Canters (2010), Fully automatic subpixel image registration of multiangle CHRIS/PROBA data, *IEEE Trans. Geosci. Remote Sens.*, *48*(7), 2829–2839, doi:10.1109/TGRS.2010.2042813.

Meroni, M., M. Rossini, V. Picchi, C. Panigada, S. Cogliati, C. Nali, and R. Colombo (2008), Assessing steady-state fluorescence and PRI from hyperspectral proximal sensing as early indicators of plant stress: The case of ozone exposure, *Sensors*, *8*(3), 1740–1754, doi:10.3390/s8031740.

Monteith, J. L. (1972), Solar-radiation and productivity in tropical ecosystems, *J. Appl. Ecol.*, *9*(3), 747–766, doi:10.2307/2401901.

Monteith, J. L. (1977), Climate and efficiency of crop production in Britain, *Philos. Trans. R. Soc. London, Ser. B*, *281*(980), 277–294, doi:10.1098/rstb.1977.0140.

Morgenstern, K., T. A. Black, E. R. Humphreys, T. J. Griffis, G. B. Drewitt, T. B. Cai, Z. Nesic, D. L. Spittlehouse, and N. J. Livingstone (2004), Sensitivity and uncertainty of the carbon balance of a Pacific Northwest Douglas-fir forest during an El Nino–La Nina cycle, *Agric. For. Meteorol.*, *123*(3–4), 201–219, doi:10.1016/j.agrformet.2003.12.003.

Myneni, R. B., and D. L. Williams (1994), On the relationship between FAPAR and NDVI, *Remote Sens. Environ.*, *49*(3), 200–211, doi:10.1016/0034-4257(94)90016-7.

Nakaji, T., H. Oguma, and Y. Fujinuma (2006), Seasonal changes in the relationship between photochemical reflectance index and photosynthetic light use efficiency of Japanese larch needles, *Int. J. Remote Sens.*, *27*, 493–509, doi:10.1080/01431160500329528.

Nichol, C. J., K. F. Huemmrich, T. A. Black, P. G. Jarvis, C. L. Walthall, J. Grace, and F. G. Hall (2000), Remote sensing of photosynthetic-light-use efficiency of boreal forest, *Agric. For. Meteorol.*, *101*, 131–142, doi:10.1016/S0168-1923(99)00167-7.

Peddle, D. R., and A. M. Smith (2005), Spectral mixture analysis of agricultural crops: Endmember validation and biophysical estimation in potato plots, *Int. J. Remote Sens.*, *26*(22), 4959–4979, doi:10.1080/01431160500213979.

Potter, C. S., J. T. Randerson, C. B. Field, P. A. Matson, P. M. Vitousek, H. A. Mooney, and S. A. Klooster (1993), Terrestrial ecosystem production: A process model-based on global satellite and surface data, *Global Biogeochem. Cycles*, *7*, 811–841, doi:10.1029/93GB02725.

Rahman, A. F., J. A. Gamon, D. A. Fuentes, D. A. Roberts, and D. Prentiss (2001), Modeling spatially distributed ecosystem flux of boreal forest using hyperspectral indices from AVIRIS imagery, *J. Geophys. Res.*, *106*(D24), 33,579–33,591, doi:10.1029/2001JD900157.

Running, S., D. Baldocchi, D. Turner, S. Gower, P. Bakwin, and K. Hibbard (1999), A global terrestrial monitoring network integrating tower fluxes, flask sampling, ecosystem modeling and EOSD satellite data, *Remote Sens. Environ.*, *70*, 108–127, doi:10.1016/S0034-4257(99)00061-9.

Schwalm, C. R., et al. (2006), Photosynthetic light use efficiency of three biomes across an east-west continental-scale transect in Canada, *Agric. For. Meteorol.*, *140*(1–4), 269–286, doi:10.1016/j.agrformet.2006.06.010.

Sellers, P. J. (1985), Canopy reflectance, photosynthesis and transpiration, *Int. J. Remote Sens.*, *6*(8), 1335–1372, doi:10.1080/01431168508948283.

Sellers, P. J., C. J. Tucker, G. J. Collatz, S. O. Los, C. O. Justice, D. A. Dazlich, and D. A. Randall (1994), A global 1° by 1° NDVI data set for climate studies. Part 2: The generation of global fields of terrestrial

biophysical parameters from the NDVI, *Int. J. Remote Sens.*, *15*(17), 3519–3545, doi:10.1080/01431169408954343.

Sellers, P. J., et al. (1995), Remote-sensing of the land-surface for studies of global change—Models, algorithms, experiments, *Remote Sens. Environ.*, *51*, 3–26, doi:10.1016/0034-4257(94)00061-Q.

Shaker, A., J. E. Nichol, and M. S. Wong (2008), Potential accuracy of image orientation of small satellites: A case study of CHRIS/PROBA data, *Photogramm. Rec.*, *23*(123), 275–289, doi:10.1111/j.1477-9730.2008.00490.x.

Staebler, R. M., and D. R. Fitzjarrald (2005), Measuring canopy structure and the kinematics of subcanopy flows in two forests, *J. Appl. Meteorol.*, *44*(8), 1161–1179, doi:10.1175/JAM2265.1.

Stylinski, C. D., J. A. Gamon, and W. C. Oechel (2002), Seasonal patterns of reflectance indices, carotenoid pigments and photosynthesis of evergreen chaparral species, *Oecologia*, *131*, 366–374, doi:10.1007/s00442-002-0905-9.

Thuillier, G., M. Herse, D. Labs, T. Foujols, W. Peetermans, D. Gillotay, P. C. Simon, and H. Mandel (2003), The solar spectral irradiance from 200 to 2400 nm as measured by the SOLSPEC spectrometer from the ATLAS and EURECA missions, *Sol. Phys.*, *214*(1), 1–22, doi:10.1023/A:1024048429145.

Toutin, T. (2004), Review article: Geometric processing of remote sensing images: Models, algorithms and methods, *Int. J. Remote Sens.*, *25*(10), 1893–1924, doi:10.1080/0143116031000101611.

Toutin, T., Y. Carbonneau, and L. St-Laurent (1992), An integrated method to rectify airborne radar imagery using DEM, *Photogramm. Eng. Remote Sens.*, *58*(4), 417–422.

Valentini, R., et al. (2000), Respiration as the main determinant of carbon balance in European forests, *Nature*, *404*(6780), 861–865, doi:10.1038/35009084.

Van Laake, P. E., and G. A. Sanchez-Azofeifa (2005), Mapping PAR using MODIS atmosphere products, *Remote Sens. Environ.*, *94*(4), 554–563, doi:10.1016/j.rse.2004.11.011.

Xiao, X. M., Q. Y. Zhang, D. Hollinger, J. Aber, and B. Moore (2005), Modeling gross primary production of an evergreen needleleaf forest using MODIS and climate data, *Ecol. Appl.*, *15*(3), 954–969, doi:10.1890/04-0470.

A. Barr, Climate Research Branch, Environment Canada, 11 Innovation Blvd., Saskatoon, SK 27N 3H5, Canada.

T. A. Black, Land and Food Systems, University of British Columbia, 2357 Main Mall, Vancouver, BC V6T 1Z4, Canada.

N. C. Coops, Forest Resources Management, University of British Columbia, 2424 Main Mall, Vancouver, BC V6T 1Z4, Canada.

F. G. Hall, A. Lyapustin, and C. J. Tucker, NASA Goddard Space Flight Center, Code 614.4, Greenbelt, MD 20771, USA.

T. Hilker, NASA Goddard Space Flight Center, Biospheric Sciences Branch Code 614.4, Bldg. 33 G310, 8800 Greenbelt Rd., Greenbelt, MD 20771, USA. (thomas.hilker@nasa.gov)

D. Y. Hollinger, U.S. Forest Service, Northeast Research Station, 271 Mast Rd., Durham, NH 03824, USA.

R. Leuning, CSIRO Marine and Atmospheric Research, GPO Box 1666, Canberra ACT, 2601, Australia.

B. Munger, Department of Earth and Planetary Sciences, 20 Oxford St., Harvard University, Cambridge, MA 02138, USA.

C. J. Nichol, School of GeoSciences, University of Edinburgh, West Mains Road, Edinburgh EH9 3JN, UK.

M. A. Wulder, Canadian Forest Service, 506 West Burnside Rd., Victoria, BC V8Z 1M5, Canada.